Talanta 93 (2012) 371–382

Contents lists available at SciVerse ScienceDirect

Talanta

journal homepage: www.elsevier.com/locate/talanta

FTIR microspectroscopy discriminates anticancer action on human leukemic cells by extracts of *Pinus kesiya*; *Cratoxylum formosum* ssp. *pruniflorum* and melphalan

Sasipawan Machana[a], Natthida Weerapreeyakul[b,*], Sahapat Barusrux[c], Kanjana Thumanu[d], Waraporn Tanthanuch[d]

[a] Graduate school, Faculty of Pharmaceutical Sciences, Khon Kaen University, Khon Kaen, 40002, Thailand
[b] Center for Research and Development of Herbal Health Product, Faculty of Pharmaceutical Sciences, Khon Kaen University, Khon Kaen, 40002, Thailand
[c] Center for Research and Development of Medical Diagnostic Laboratories, Faculty of Associate Medical Sciences, Khon Kaen University, Khon Kaen, 40002, Thailand
[d] Synchrotron Light Research Institute (Public Organization), Nakhon Ratchasima, 30000, Thailand

ARTICLE INFO

Article history:
Received 7 January 2012
Received in revised form 21 February 2012
Accepted 22 February 2012
Available online 1 March 2012

Keywords:
Apoptosis
Pinus kesiya
Cratoxylum formosum ssp. *pruniflorum*
Melphalan
FTIR microspectroscopy

ABSTRACT

Apoptosis is the principal molecular goal of chemotherapeutics for effective anticancer action. We studied the effect of 50% ethanolic-water extracts of *Pinus kesiya*, *Cratoxylum formosum* ssp. *pruniflorum* and melphalan on cytotoxicity and apoptosis induction for human leukemic U937 cells, and explored the mode of action using FTIR microspectroscopy. The number of viable U937 cells *in vitro* was decreased in a concentration-dependent manner by all tested compounds, although potency differed between the U937 and Vero cells. Melphalan and the extract of *C. formosum* exhibited relatively lower IC_{50} values (15.0 ± 1.0 and 82.7 ± 3.2 μg/mL respectively) and higher selectivity (selective index > 3) than the extract of *P. kesiya* (299.0 ± 5.2 μg/mL; selective index < 3) on the U937 cells. All three compounds significantly induced apoptosis through the late stage – seen by the indicative DNA ladder – with the most effective being melphalan, then the *P. kesiya* and *C. formosum* extracts. FTIR microspectroscopy revealed that all three compounds raised the intensity of the β-pleated sheet – higher than that of the untreated U937 cells – corresponding to a shift in the α-helix band associated with an alteration in the secondary structure of the protein band, confirming induction of apoptosis via pro-apoptotic proteins. The differences in intensity of the FTIR bands associated with lipids, proteins and nucleic acids were responsible for discrimination of the anticancer mode of action of each of the three compounds. The FTIR data suggest that the two plant extracts possessed anticancer activity with a different mode of action than melphalan.

1. Introduction

Cancer is a non-communicable disease and the second leading cause of death in the world [1]. Carcinogenesis is multifactorial and complex; especially the mechanisms deregulating oncogenes and tumor suppressor genes [2]; wherein normal cells are modified to cancer cells, characterized by uncontrolled growth and metastasis [2]. Researchers have found that these modifications also confer a greater capacity to survive exposure to varieties of toxic stresses, including those from anticancer agents [3]. Generally, new drugs are evaluated for their potential to kill cancer cell lines. This approach, however, is insufficient, and molecules with new modes of action are required.

Programmed cell death (or apoptosis) is an autonomous process wherein cells are dismantled; thereby removing individual damaged components of an organism, without destroying or damaging the organism [4]. Since the apoptotic body has been rapidly removed by macrophages, the inflammatory process has been avoided so that it is described as a clean process [5]. The anticancer activity involving induction of apoptosis has been used as a new therapeutic strategy and/or for investigating the anticancer activity of various compounds [6].

Common biochemical events of a cell undergoing apoptosis include: changes in the cell membrane potential; altered levels of protein and RNA biosynthesis; and degradation of DNA into small fragments. DNA fragmentation, activation of caspases and externalization of phosphatidylserine are considered the hallmarks

* Corresponding author at: Center for Research and Development of Herbal Health Product, Faculty of Pharmaceutical Sciences, Khon Kaen University, Khon Kaen, 40002, Thailand. Tel.: +66 43 202 378; fax: +66 43 202 379.
E-mail addresses: sasipawan.machana@gmail.com (S. Machana), natthida@kku.ac.th, nweera@hotmail.com (N. Weerapreeyakul), sahapat@kku.ac.th (S. Barusrux), kanjanat@slri.or.th (K. Thumanu), waraporn@slri.or.th (W. Tanthanuch).

0039-9140/$ – see front matter © 2012 Elsevier B.V. All rights reserved.
doi:10.1016/j.talanta.2012.02.058

of apoptosis [7]. The observed morphological changes of apoptotic cells include: membrane blebbing, cell shrinkage, nuclear condensation, fragmentation and packaging of cellular material into apoptotic bodies. These morphological changes can be assessed by phase contrast, fluorescence and scanning electron microscopy (SEM) [8]. The late-stage of apoptosis is DNA laddering, characterized by DNA fragmentation, detectable by agarose gel electrophoresis [8].

The aforementioned methods are used to screen for changes in apoptotic cells with specific DNA changes but each needs specific reagents, complicated sample handling and/or highly trained personnel. Moreover, the high throughput, highly sensitive screening assays (*i.e.*, DNA microarray and proteomic assay) that are used to investigate the mode of action of each drug (or how compounds contribute to cell apoptosis) are beyond the practical capability of conventional labs [9].

Fourier Transform Infrared (FTIR) spectrum yields a precise image of all the chemical bonds present in the cells with the least complicated and most expedient methods of sample handling. FTIR microspectroscopy is a well-known sensitive tool and cheaper than the high throughput assays for the analysis of biochemical composition of cells or tissues such as carbohydrates, lipids, proteins and nucleic acids [10]. FTIR spectra also account for the conformations and pick up the secondary protein structure [11]. FTIR has been used to generate the fingerprint of entire biochemical changes in biological samples [9,12]; to classify bacteria genera, species and strains [13]; to characterize the mode of action of the investigated therapeutic agent on differentiation, proliferation, apoptosis and/or cell cycle of different cell lines and tissues [12]. FTIR might therefore be adapted as an alternative method for assessing the mode(s) of action of prospective compounds.

Our study examined the anticancer activity of crude plant extracts from – *Pinus kesiya* and *Cratoxylum formosum* ssp. *pruniflorum* – against the human leukemic cell line U937 vs. the positive control drug, melphalan. The anticancer activity was investigated for (a) cytotoxic effect against U937 using a neutral red assay and (b) the induction of apoptosis by evaluation of morphological changes in nuclei after DAPI staining and DNA fragmentation using agarose gel electrophoresis. The cancer cells that responded to the test compounds were also probed using FTIR spectroscopic analysis. These experiments provided a preliminary evaluation of the efficacy, toxicity and mode of anticancer action of the test compounds.

2. Materials and methods

2.1. Chemicals and reagents

The organic solvents used for extraction were of analytical grade from Fisher Scientific (UK) and Labscan (Thailand). Acetonitrile (HPLC grade, Fisher Scientific, UK), *Ortho*-phosphoric acid (analytical grade, BHD, England) and ultrapure water from Milli-Q system (Millipore, Bedford, USA) were used for the mobile phase preparation. The standard agents and melphalan were provided by Sigma–Aldrich Chemie GmbH (Eschenstr. Taufkirchen, Germany). The reagents used in the cell assay were of molecular biological grade. Dimethyl sulfoxide (DMSO) was bought from United States Biological (Swampscott, Massachusetts (MA), USA). The reagent and culture media Dulbecco's modified Eagle's medium (DMEM) were bought from GIBCO®, Invitrogen Corporation (USA). Sodium bicarbonate ($NaHCO_3$) and the fluorescence dye 4′,6-diamidino-2-phenylindole (DAPI) were purchased from Sigma–Aldrich Chemie GmbH (Eschenstr. Taufkirchen, Germany). Neutral red and a standard anticancer drug (melphalan) were purchased from Sigma Chemical Co. (USA). Sodium chloride (NaCl) was purchased from Ajax Finechem (Auckland, New Zealand).

2.2. Plant material and extractions

Both *C. formosum* ssp. *pruniflorum* and *P. kesiya* were collected between 2008 and 2009 from Chaiyaphum province, Thailand, and were visually authenticated according to taxonomy. The Herbarium collection was kept at the Center for Research and Development of Herbal Health Products (CRD-HHP), Khon Kaen University, Thailand. Each of the dried plants – *C. formosum* ssp. *pruniflorum* (TT-OC-SK-862, twig) and *P. kesiya* (TT-OC-SK-910, branch) – were cut and macerated with 50% ethanol and water in a ratio of 1 g to 6 ml for 7 d with occasional shaking. The solvent was (a) filtered (b) distilled *in vacuo* using a rotary evaporator below 40 °C and (c) freeze-dried to obtain the crude extracts. The respective percent yields of the extracts from *C. formosum* and *P. kesiya* were 3.78% and 4.26% dried weight. The stock solution of the crude extracts was freshly prepared by dissolving them in dimethyl sulfoxide (DMSO).

2.3. Cell culture

Human leukemic U937 cancer cells were cultured in RPMI-1640 medium. The normal cells of African green monkey kidney epithelial Vero cells were cultured in DMEM medium (Gibco, Grand Island, NY), containing 10% fetal bovine serum, 100 U/ml penicillin and 100 mg/ml streptomycin; incubated at 37 °C in a humidified atmosphere containing CO_2 level (5%).

2.4. Neutral red assay

The cytotoxic activity of the plant crude extracts in the U937 and Vero cell lines were assessed using the neutral red assay. The neutral red dye accumulated in the lysosomes of viable and uninjured cells. Briefly, the respective suspension seeding density for the human leukemic U937 and normal Vero cells was 5×10^5 and 3×10^5 cells. These were put in 96-well plates and incubated for 24 h. Afterward, the cells were treated with various concentrations of the solution of the crude plant extracts or melphalan in DMSO and incubated for an additional 24 h. The maximum final concentration of the compound was 500 μg/mL in order to maintain a 1% v/v DMSO with a cytotoxicity < 10% compared to the untreated cells. Then the cells were directly stained with a final concentration of 50 μg/mL neutral red dye and incubated for another 2 h. The neutral red stained viable cells were dissolved by using 0.33% HCl in isopropanol and detected by colorimetry. Absorbance was measured at 520 nm and 650 nm (reference wavelength) using a spectromicroplate reader. All experiments were replicated five times. The percentage of cell cytotoxicity was calculated and the concentration causing 50% cell death (IC_{50}) was determined from a linear equation obtained from the plot between the percentage of cell cytotoxicity vs. the compound concentrations. The Selectivity Index (SI) of melphalan and the crude plants extracts were compared with the IC_{50} for the Vero cells divided by the IC_{50} for the U937 cells.

2.5. DAPI staining assay

Apoptosis was determined by a fluorescence dye employing DAPI to identify the condensation and fragmentation of nuclear DNA [14]. Briefly, the cell density of the U937 was 1×10^5 cells, which were seeded in 24-well plates and incubated for 24 h prior to incubation with the test compound. The U937 cells were treated with approximately $2 \times IC_{50}$ concentration of the compound for 24 h. The respective concentration used for melphalan and *C. formosum* was 30 μg/mL and 165 μg/mL, except for *P. kesiya* for which the concentration was 500 μg/mL to keep the % DMSO less than 1%. The culture medium was removed and washed using fresh medium and the cells fixed by cold methanol. The DAPI dye was then added to stain the nuclear DNA for 1 h. The excess dye was removed and

PBS:Glycerin (1:1) added. The DAPI staining assay was replicated thrice in independent experiments. The pictures of DAPI staining were captured using the inverted fluorescence microscope. The average %apoptotic cells were calculated from three independent wells with 10 eye views in each well under the inverted fluorescence microscopy at a magnitude of 40×.

2.6. Determination of DNA fragmentation

The DNA fragmentation – an indicator of late-stage apoptosis – occurs because of DNase activity cleaving chromatin at the boundaries between the nucleosomes; generating areas of high molecular weight (>50 kbp) and nucleosome-sized (200 bp) DNA fragments that can be observed as ladders, by gel electrophoresis [15]. Briefly, after the cancer U937 cells were treated with the test compounds for 24 h (melphalan = 30 μg/mL; *C. formosum* = 165 μg/mL; and *P. kesiya* = 500 μg/mL). The U937 cells were collected and washed with fresh medium. The U937 cell suspension was then transferred to a microcentrifuge tube and centrifuged at 300 × *g* for 5 min and the resultant cell pellet collected. The DNA in the cell pellet was extracted using a QIAGEN kit and the resulting 2 μg of DNA analyzed by electrophoresis on 2% agarose gels containing 0.1 mg/mL ethidium bromide (Sigma). The DNA was mixed with loading dye and the gel electrophoresed in 0.5% TBE buffer at 250 V for 1 min and 20 V for 4 h. After electrophoresis, the DNA fragment was analyzed using InGenius L gel documentation (Syngene, USA) and a picture of the electrophoresis gel taken.

2.7. FTIR microspectroscopy

Cancer cells treated with the test compounds at the same concentration used in DAPI staining assay for 24 h were washed with 0.9% NaCl, deposited onto an indium tin oxide-coated, silver-doped glass slide (MirrIR, Kevley Technologies) then vacuum dried for 10 min in the desiccator [16]. The cells on the slide were rinsed for few seconds with distilled water and vacuum dried for 10 min in the desiccator. This step was repeated thrice. The washed and dried cells were kept in a desiccator until used.

Biomolecular changes in the cell samples were determined using the FTIR microspectroscopy technique. Measurements were performed on the off-line IR spectroscopy facility, at the Synchrotron Light Research Institute (Public Organization), Thailand. The Bruker Hyperion 2000 microscope (Bruker Optics Inc., Ettlingen, Germany) – equipped with a nitrogen cooled MCT (HgCdTe) detector with a 36 × IR objective – coupled to a Bruker Vertex 70 spectrometer was used for FTIR data acquisition. The FTIR spectra were obtained in the reflection mode, collecting 64 scans, 68 μm × 68 μm aperture size at a resolution of 4 cm^{-1} over a measurement range of 4000–600 cm^{-1}. Spectral acquisition and instrument control were performed using OPUS 6.5 software (Bruker Optics Ltd, Ettlingen, Germany).

Principal Component Analysis (PCA) (with a spectral range of 3000–2800 cm^{-1} and 1790–900 cm^{-1}) were performed using the Unscrambler software (version 9.7, CAMO Software AS, Oslo, Norway) for identification of a significant variation between the data sets. Data manipulations were processed by taking the second derivative using the Savitzky–Golay algorithm (with nine points of smoothing allowing minimization of the effects of variable baselines) and normalized with extended multiplicative signal correction (EMSC), which normalizes spectra, accounting for differences in sample thickness and correcting for scattering artifacts. Six principal components (PCs) were chosen for analysis. Score plots (2D) and loading plots were used to display the clustering and variations in the data set, respectively.

The peak areas of integration were done using OPUS 6.5 software. The integrated peak area of lipids (3000–2800 cm^{-1}) and nucleic acids (1300–950 cm^{-1}) were used and represented on a Histogram. The Amide I spectra (1700–1590 cm^{-1}) were acquired for differentiation of the protein structure by using a curve fitting analysis of each of the cell lines. The spectra were processed by taking the second derivative from the average of all of the spectra as per the Savitzky–Golay algorithm with 13 points of smoothing and EMSC.

Unsupervised hierarchical cluster analysis (UHCA) of the FTIR spectral data sets was performed using Ward's algorithm; which utilizes a matrix defining the inter-spectral distances to identify the two most similar FTIR spectra. The spectral distances between all of the remaining spectra and the new clusters were then recalculated. UHCA was performed using OPUS 6.5 software (Bruker) using the spectral regions from 3000–2800 cm^{-1} to 1750–900 cm^{-1}.

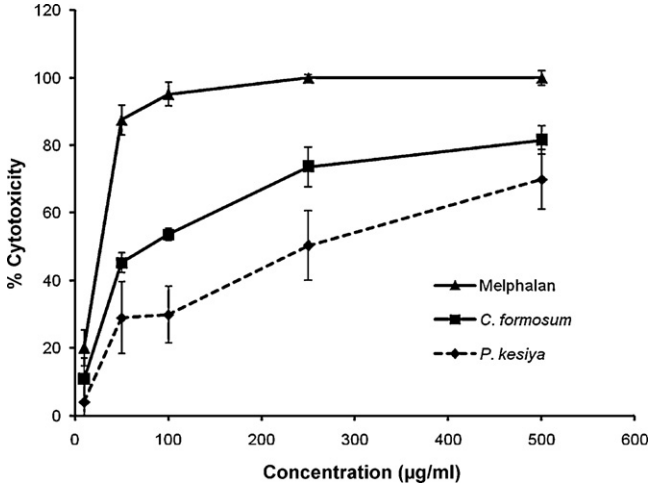

Fig. 1. Effect of crude plant extract on U937 cell line for 24 h. IC_{50} calculated and shown in Table 1.

2.8. Statistical analysis

SPSS was used to compare the peak areas of integration of the biological bands of lipids and the nucleic acid bands between the U937-untreated and -treated cells using a One-way ANOVA test. Multiple comparisons were analyzed using Tukey-HSD test ($P < 0.05$).

3. Results and discussion

3.1. Cytotoxicity induced by 50% ethanol–water extract of C. formosum, P. kesiya and melphalan

The 50% ethanol–water extracts of *C. formosum* and *P. kesiya* exhibited cytotoxicity in a dose-dependent manner upon the human leukemic U937-cell line (Fig. 1). The cytotoxicity and selective indices of the crude plant extracts compared to melphalan are presented in Table 1. The extracts from both *C. formosum* and *P. kesiya* were found to possess cytotoxicity against U937 cells. The

Table 1
Cytotoxic activity of plant crude extracts and melphalan drug against cancer cell lines.

Plant samples	Part used	IC_{50} (μg/mL) ± SD		Selective index
		U937	Vero	
P. kesiya	Branch	299.0 ± 5.2	>500	>1.7
C. formosum	Twig	82.7 ± 3.2	>500	>6.0
Melphalan	–	15.0 ± 1.0	59.9 ± 3.2	>4.0

extract of *C. formosum* exerted higher selectivity to the U937 cells than melphalan.

3.2. Apoptosis induced by 50% ethanol–water extract of C. formosum, P. kesiya and melphalan

The morphological changes of apoptotic nuclei were clearly observed under the inverted fluorescence microscope (after DAPI staining), after the U937 cells were exposed to the crude plant extracts for 24 h (Fig. 2). In the control group (untreated cells), the nuclei were roundish and homogenously stained by DAPI; whereas, the apoptotic nuclei in the treated U937 cells were polygonal, small, detached and having apoptotic body characteristics (Fig. 2). Melphalan was found to induce a significantly greater percentage of apoptosis than the crude plant extracts with $72.8 \pm 10.2\%$ apoptotic cells ($P < 0.05$). The extract from *P. kesiya* exhibited $65.5 \pm 8.2\%$ apoptotic cells, whereas the extract from *C. formosum* exhibited $48.8 \pm 8.1\%$ apoptotic cells. The cytotoxic effect leads to death of the cancer cells – either by apoptosis or necrosis at variable rates. Notably, the high cytotoxic *C. formosum* extract exhibited a lower % apoptosis than the low cytotoxic *P. kesiya* extract: it may be that the *C. formosum* extract induced more necrotic death in addition to apoptosis than the *P. kesiya* extract.

DNA fragmentation – the hallmark of late-stage apoptosis – is used to confirm biochemical change in the cells undergoing apoptosis [7]. Our results showed that, as with melphalan, both of the crude extracts (at $2 \times IC_{50}$ concentrations) induced fragmentation of DNA after a 24 h exposure (Fig. 3); suggesting that both have anticancer characteristics.

3.3. Identification of IR spectra in U937 cells to explore anticancer mode of action of plant extracts and melphalan

We found that melphalan and the extracts of *P. kesiya* and *C. formosum* all possessed anticancer activity against the human leukemic U937 cells, by inducing late-stage apoptosis. Since different drug targets yield different infrared fingerprints, the infrared spectrum of cells exposed to the anticancer drug provides a precise image of the chemical bonds present, revealing characteristics of the mode of action of the therapeutic agent under investigation [13]. FTIR analysis was therefore adapted in our study to explore the anticancer mode of action of the plant extract vs. melphalan.

FTIR spectra of the U937 cells in the absence and presence of the test compounds were acquired in the range of 4000–600 cm^{-1} (Fig. 4A). The infrared spectra profile of the U937 cells under the four different conditions were similar (Fig. 4A) and can be divided into three regions: (1) the lipid region (2) the proteins region and (3) carbohydrates and nucleic acids.

(1) The lipid region (3000–2800 cm^{-1}) is assigned to the symmetrical and asymmetrical stretching vibrations of the CH_2- and CH_3- groups contained in the fatty acids of the cells [17,18]. The 1800–1700 cm^{-1} region is characteristic of the ester C=O stretching of the lipid head-group [13]. The 1478 cm^{-1} and 1350 cm^{-1} region is characteristic of the CH_3-, CH_2-bending of the methylene chains in lipids [17].
(2) The protein region (1700–1300 cm^{-1}) is assigned to the amides I and II. The amide I band (1700–1500 cm^{-1}) indicates a secondary structure of protein absorption. The stretching of the carbonyl from the peptide bond was observed at 1650 cm^{-1}

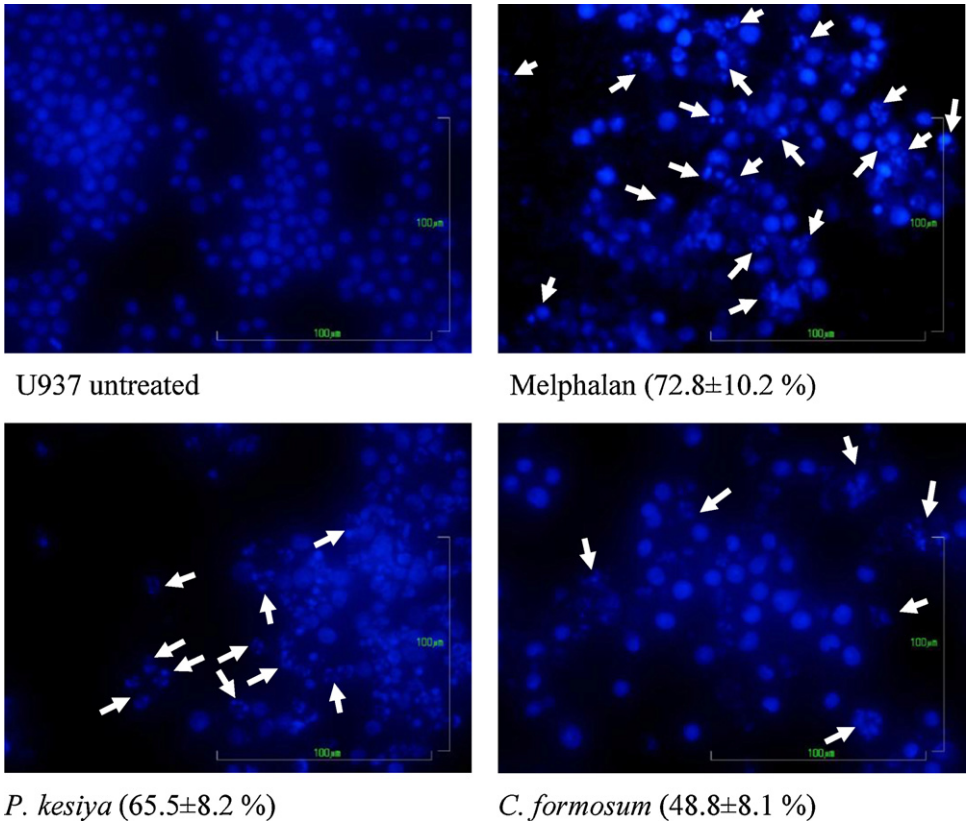

Fig. 2. Morphology of nuclear DNA stained with a DAPI dye under inverted fluorescence microscopy. (A) Control (or untreated) U937 cell line: nuclear DNA roundish. (B)–(D) apoptotic cells (indicated by arrows): nuclear DNA became polygonal, small, detached or sparse, membranous frothed and wizened after treatment with melphalan, *P. kesiya* and *C. formosum*, respectively.

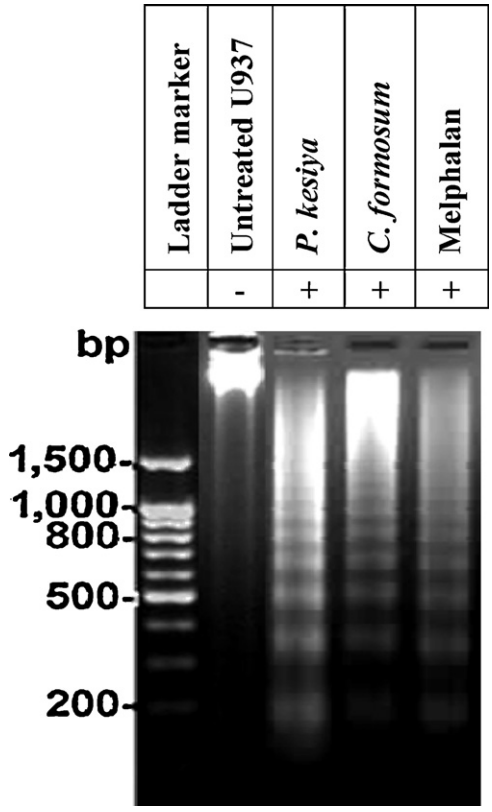

Fig. 3. DNA ladder in U937 cell line. DNA ladder was detected in U937 cell line after treatment with *P. kesiya* extracts (500 μg/mL), *C. formosum* extracts (165 μg/mL) and melphalan (30 μg/mL) for 24 h.

(amide I). The deformity of the protein at the amide II of N–H bending and C–N stretching was observed at 1540–1500 cm^{-1}. The bands between 1480 and 1300 cm^{-1} are represented by amino acid side chains and fatty acids [13,17].

(3) The carbohydrate and nucleic acid region (1300–900 cm^{-1}) is assigned to the absorptions resulting from the carbohydrates and phosphates mainly associated with nucleic acids, i.e., DNA and RNA. The absorption bands at 1240 cm^{-1} and 1085 cm^{-1} are characteristic of the asymmetrical and symmetrical phosphodiester vibrations of nucleic acids. The C–O bond of glycogen and other carbohydrates are overlapped between 1150 cm^{-1} and 1020–1025 cm^{-1} [17–19]. The RNA ribose chain and C–C bond of nucleic acids faintly appear at 966 cm^{-1} [20,21].

Over hundred FTIR spectra were obtained from each sample conditions. The high-quality FTIR spectra were generated by PCA analysis on each data set for selecting the representative spectra for further analysis, discarding the out group spectra. The selected spectra of each condition were performed averaging. The average spectrum of all four conditions were combined and done for vector normalization. The average FTIR spectra from each data set presented similar pattern, containinglipids, proteins and nucleic acids profile (Fig. 4A). The peak area integration of each biological molecule was carried out presenting significant differences between the untreated and treated U937 cells (Fig. 4B) as follows:

3.3.1. Nucleic acids and carbohydrate region

The weak peaks of treated U937 cells observed in the nucleic acids and carbohydrates region decreased at: (a) 1394 cm^{-1} (which was assigned to symmetric vibrations of carboxylate functional groups of amino acid side chains and fatty acid); (b) 1234 cm^{-1} (assigned to $\nu_{as}PO^{2-}$); (c) 1170 cm^{-1} (assigned to νC–O); (d) 1085 cm^{-1} (assigned to $\nu_{s}PO^{2-}$); (e) 1052 cm^{-1} (assigned to C–O vibration from glycogen and other carbohydrates); and, (f) 966 cm^{-1} (assigned to C–C/C–O stretching of deoxyribose–ribose vibration) [21,23] (Fig. 4B). These partitions are based on the assumption that the dramatic decrease of nucleic acids (DNA, RNA base) regions – after U937 cells were treated with melphalan, *C. formosum* and *P. kesiya* – were caused by apoptosis processes. This assumption agrees with a previous report on apoptosis observed in U937 [18]. The anticancer mechanism of melphalan is an alkylating activity associated with the cross-linking of DNA double strands which induces DNA strand breaks leading to apoptotic cell death [24]. By way of corroboration, a decrement of nucleic acids was observed after the U937 cells were treated with the crude plant extract of *C. formosum* and *P. kesiya*, just as happened with cells treated with melphalan. Thus, the FTIR spectra reflect a decrease in the nucleic acids region when melphalan, *C. formosum* and/or *P. kesiya* induce U937 cells to die via the apoptosis pathway. It has been reported that the decrease in the nucleic acids region (1300–900 cm^{-1}) in apoptotic cells was related to DNA degradation [18]. This DNA spectral feature is a uniquely useful parameter for characterization of the death mode because it has been found to decrease during apoptosis and, by contrast, to increase during necrosis [18]. The apoptotic DNA absorbs less IR due to DNA opaqueness (non-Beer-Lambert absorption) as a consequence of DNA condensation; despite DNA degradation during apoptosis [18]. The opaque nature of the apoptotic chromatin is due to its tight association with HMGB-1, which masks the chromatin from neighboring cells and prevents activation of the inflammatory response. To compare, during necrosis the DNA is degraded but not compacted; hence, the necrotic DNA becomes less opaque and absorb more IR [18]. Additionally, it was reported that the DNA is completely unwound in necrotic cell death; thus, 100% of the DNA is visible to IR [18].

3.3.2. Lipid region

The lipid regions (3000–2800 cm^{-1} $\nu_{s}CH_2$ and $\nu_{as}CH_2$ stretching (2852, 2923 cm^{-1}), $\nu_{as}CH_3$ (2975 cm^{-1}), C=O (1755–1710 cm^{-1}), CH_3, CH_2 (1478–1350 cm^{-1})) showed a significant increase in the melphalan-treated vs. the untreated U937 cells ($P < 0.05$, one-way ANOVA); while those treated with the extracts of *C. formosum* and *P. kesiya* exhibited a decrease (Fig. 4B).

When cells undergo apoptosis, there will be a phosphatidylcholine flip-flop across the plasma membrane and a transfer to the outer surface [18,22]. The increase of lipids in the apoptotic cells is reported to be a consequence of the membrane changes – related to phosphatidylserine exposure, membrane blebbing and vesicle formation – leading to an increase of methylene absorbance [18]. To contrast, the changes in the membrane due to necrosis typically include swelling of cellular organelles and loss of plasma membrane integrity; leading to a decrease of the lipid membrane [18]. It has, however, been reported that the use of lipid absorbance alone is insufficient evidence for distinguishing between apoptosis and necrosis [18].

The predominant spectral increment of lipids emitted by the melphalan-treated cells compared to the untreated cells suggests that there has been an alteration in the lipid membranes associated with apoptosis such as by phosphatidylserine exposure [18,22]. Interestingly, although our results show that the test compounds might induce cells to advance to a different stage of apoptosis, this type of apoptosis induction did not result in a significantly different lipid spectra than that emitted by the untreated cells. It implies that lipid absorbance is not a good marker for identify apoptosis.

To illustrate, a histogram was generated to display the mean integrated areas of original spectra for lipid regions at 3000–2800 cm^{-1} (δCH_2), 1760–1724 cm^{-1} (νC=O),

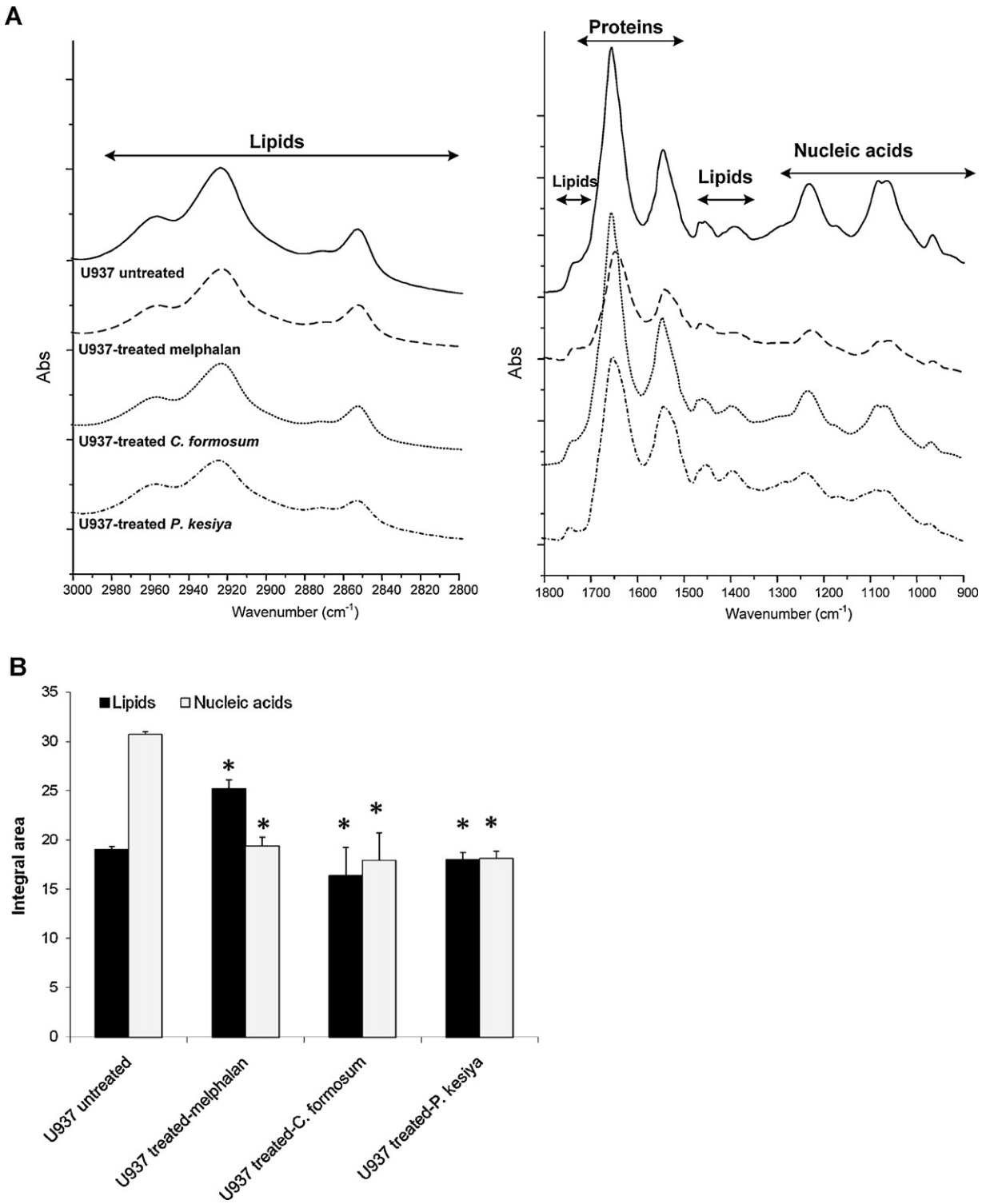

Fig. 4. Analysis of untreated and treated-U937 cells using FTIR spectroscopy. (A) Average FTIR spectra ($n = 260$) obtained from human leukemic U937 cells under 4 different conditions: original IR spectra of untreated U937 cells ($n = 87$) (solid), U937-treated with melphalan ($n = 54$) (dashed), *C. formosum* ($n = 55$) (dotted) and *P. kesiya* ($n = 64$) (dash-dot). The lipid, proteins and nucleic acid regions are identified. (B) Histogram shows mean integrated areas for remarkable lipid and nucleic acid regions of original spectra. Differences between means of areas for both regions were significantly different (*) between untreated and treated U937 cells with melphalan, crude extract of *C. formosum* and *P. kesiya* with $P < 0.05$, by one-way ANOVA. Error bars indicate standard errors of means (untreated, $n = 87$; melphalan, $n = 54$; *C. formosum*, $n = 55$; and *P. kesiya*, $n = 64$).

1478–1350 cm^{-1} (δCH_2, CH_3) and nucleic acid regions at 1300–900 cm^{-1} (Fig. 4B). The histogram showed differences at the lipid and nucleic acid levels of treated cells compare to untreated cells. These biochemical changes – observed from lipid and nucleic acid contents – were influenced by melphalan more than by the extracts of *P. kesiya* and *C. formosum* (Fig. 4B). The different FTIR spectra of the lipid and nucleic acid regions in the U937 cells treated with melphalan, *C. formosum* and *P. kesiya* might be caused by differences in cell responses related to the death mode of action.

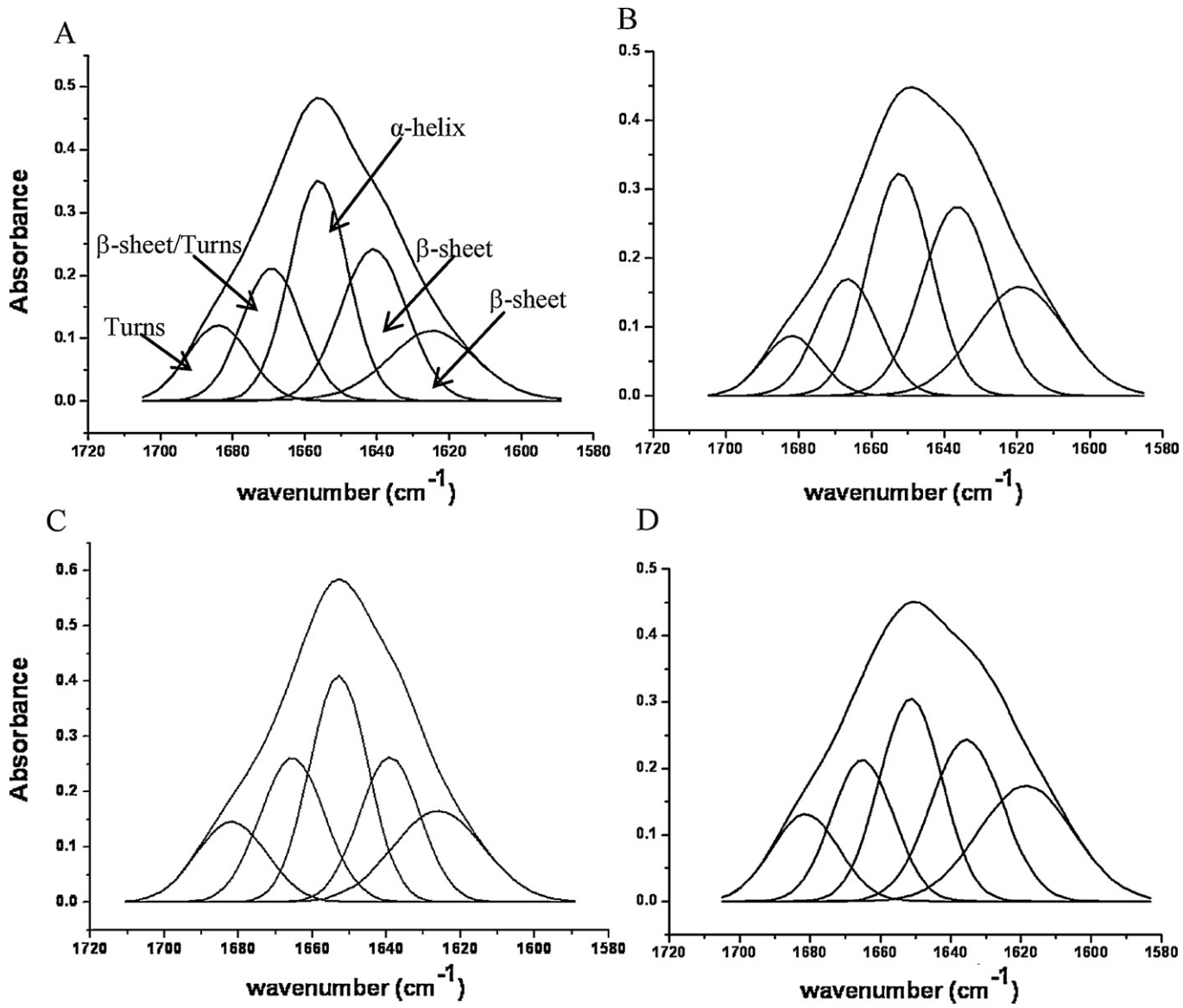

Fig. 5. Absorbance of amide I band contour with best-fit 50% Loentzian/Gaussian individual component bands for U937-untreated (RMS error is 0.004050) (A), U937-treated with melphalan (RMS error is 0.003502) (B), *P. kesiya* (RMS error is 0.003769) (C) and *C. formosum* (RMS error is 0.004063) (D).

3.3.3. Protein region

The FTIR spectra of protein regions have two prominent features, the amide I (1700–1590 cm^{-1}) and the amide II (1560–1500 cm^{-1}) bands, which arise primarily from the C–O and C–N stretching vibrations of the peptide backbone, respectively [25,26].

To gain more information, the positions and integral area of the FTIR spectra in the protein region were performed and the resulting differences in spectra between the untreated and treated U937 cells compared using curve fitting to predict the protein's secondary structure. After calculating the average original spectra of the amide I band (1700–1590 cm^{-1}) in the treated and untreated U937 cells, the changes observed in the amide I band shape of the treated cells could be divided into five components (Fig. 5): the 1st and 2nd components with a respective peak range of between 1618 and 1628 cm^{-1} and 1635–1641 cm^{-1} were assigned to the β-pleated sheet; the 3rd component between 1650 and 1656 cm^{-1} was associated with the presence of an α-helix secondary structure; while for the 4th and 5th peak positions, the respective presence of the β sheet and turn structures was represented by the peak range of between 1665 and 1670 cm^{-1} and 1680–1685 cm^{-1} [18–23] (Table 2 and Fig. 5). After the curve fitting computations of the average spectrum for each incubation condition, the differences between mean pairs were determined using a one-way ANOVA ($P < 0.05$, Tukey-HSD) (Table 2). The integral area of the β-sheet structure (1618–1628 cm^{-1}) of the U937 cells after being treated with melphalan (20.8%), *C. formosum* (18.3%) and *P. kesiya* (22.0%) showed higher intensity than the untreated U937 cells (15.9%) (Table 2). Furthermore, these β-sheet structures were significantly shifted from 1625 cm^{-1} in the untreated U937 cells to 1619 cm^{-1} and 1618 cm^{-1} in the melphalan- and *P. kesiya*-treated U937 cells, respectively (Table 2). The integral area of the α-helix structure of the U937 cells after being treated with melphalan (29.1%), *C. formosum* (29.1%) and *P. kesiya* (25.3%) resulted in a lower intensity than the untreated-U937 cells (30.3%) (Table 2). Moreover, the α-helix structure was significantly shifted from 1656 cm^{-1} in the untreated U937 cells to 1652–1651 cm^{-1} after the U937 cells were treated with melphalan, *C. formosum* and *P. kesiya* (Table 2). The spectra from other positions in the cancer cells showed the same number of overlapping bands with very small differences in their positions.

Table 2
The positions and integral area of proteins assignments of U937 untreated and after treated with melphalan, *C. formosum* and *P. kesiya* extracts.

Assignment	Untreated		Melphalan		*C. formosum*		*P. kesiya*	
	Position (cm^{-1})	Integral area (%)	Position (cm^{-1})	Integral area (%)	Position (cm^{-1})	Integral area (%)	Position (cm^{-1})	Integral area (%)
β-sheet	1625	15.9	1619[b]	20.8[a]	1626	18.3[a]	1618[b]	22.0[a]
β-sheet	1641	23.9	1636[b]	28.0[a]	1639	19.5[a]	1635[b]	23.3
α-helix	1656	30.3	1652[b]	29.1[a]	1652[b]	29.1[a]	1651[b]	25.3[a]
Turns	1669	18.8	1666	14.9[a]	1665	20.5[a]	1665	17.5[a]
Turns	1684	11.1	1682	7.2[a]	1681.9	12.5[a]	1681	11.8

[a] Means the integral area was statistically significant difference from the untreated U937 cells ($P < 0.05$, one-way ANOVA).
[b] Means the peak position was statistically significant difference from the untreated U937 cells ($P < 0.05$, one-way ANOVA).

The alteration of protein structures in apoptotic cells was previously observed among the Bcl-2 family and Bax – members of the apoptotic proteins death-promoting group [27]. The Bcl-2 protein family comprises pro-apoptotic (i.e., Bax and Bid) and anti-apoptotic proteins (*i.e.*, Bcl_2), which play important roles in the regulation of apoptosis. The Bax protein is involved in the permeabilization of the outer mitochondrial membrane (OMM), forming ion channels, inducing the translocation of the cytochrome c from the mitochondrial intermembrane space to the cytoplasm, thereby activating proteolytic proteins (caspases) and finally apoptosis [28].

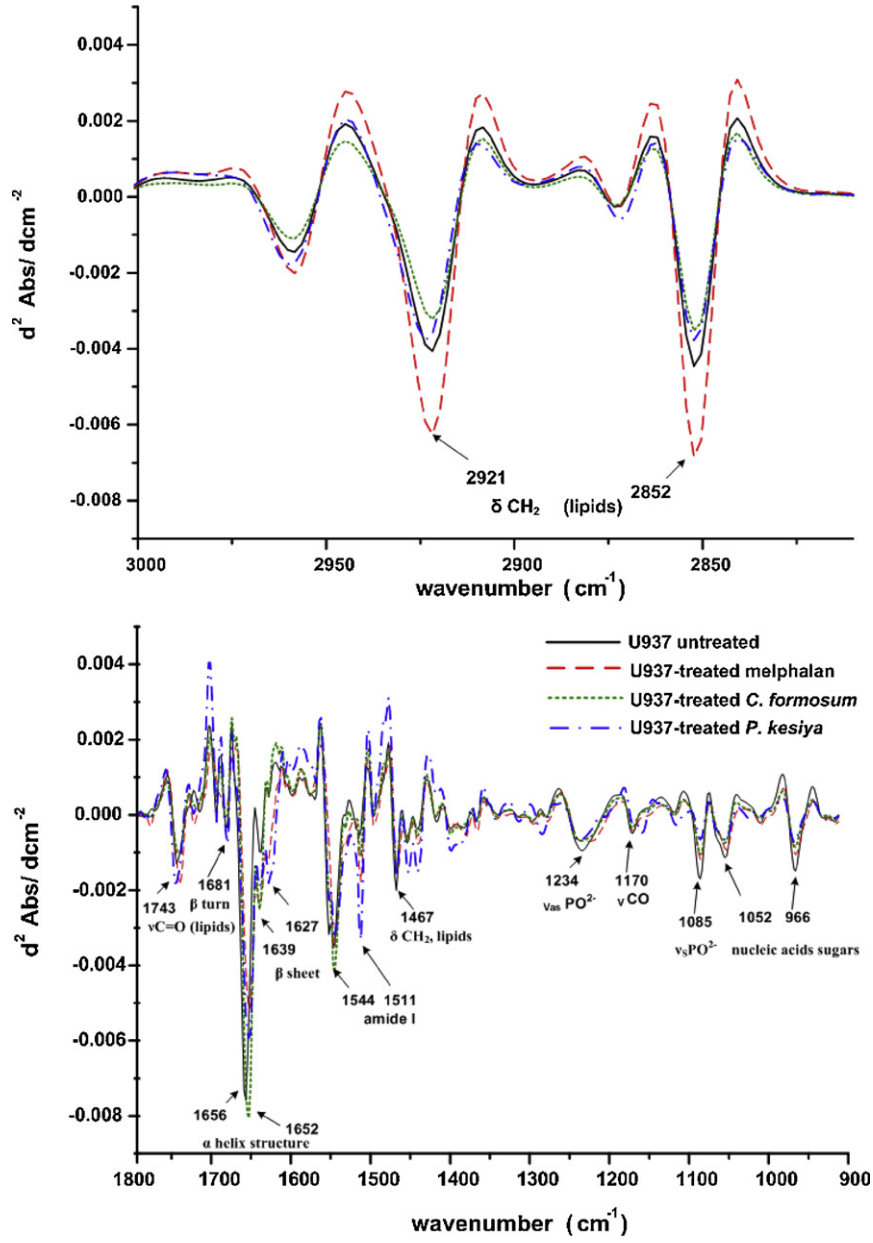

Fig. 6. Average 2nd derivative spectra from experiments (for untreated cells, $n = 87$; melphalan-, $n = 54$; *C. formosum*-, $n = 55$; and *P. kesiya*-treated cells, $n = 64$) after baseline and normalized with extended multiplicative signal correction (EMSC) and represented in three different regions: lipids (3000–2800 cm^{-1}), protein (1700–1500 cm^{-1}) and nucleic acid region (1400–940 cm^{-1}). Prominent bands in spectra assigned to functional group vibrations and corresponding macromolecular classes.

The electrostatic interaction of the C-terminal domain of Bax with the mitochondrial membrane induces a transition from an intermolecularly hydrogen-bonded β-pleated sheet (1620 cm^{-1}) to a pro-apoptotic protein (Bax protein) [29].

Monitoring the overall changes occurring in the U937 cells upon exposure to different test compounds is a complex mechanism. To more precisely compare the peak positions of the original spectral range visually, the spectra were processed by taking a second derivative, which better resolved the overlapping peaks of the original spectra (Fig. 6). The scattering artifacts were reduced by using the Extended Multiplicative Scatter Correction (EMSC), which presented the second derivative spectra of nucleic acids, lipid and protein regions in the U937 cells after being treated with melphalan, *C. formosum* and *P. kesiya* vs. the U937-untreated cells. The correlated difference is presented in Fig. 6.

Fig. 6A and B illustrated the second derivative data of the respective lipid region and nucleic acid and protein regions of the cell samples under the four conditions studied. These results support Figs. 4 and 5. Importantly, the second derivative spectra allow the identification of various secondary structures that exist in the protein. In the untreated U937 cells, the α-helix band component at 1656 cm^{-1} was observed and was found to shift to the same peak position at 1652 cm^{-1}, after the cells were exposed to the three test compounds. The most dramatic increase in intensity at 1652 cm^{-1} was observed in the *C. formosum*-treated U937 cells, which was higher than the *P. kesiya* extract and melphalan, respectively. The β-sheet band component (1639 cm^{-1}) in the untreated U937 cells was observed to have a low intensity, which gradually increased when the cells were treated with melphalan and the *P. kesiya and C. formosum* extracts. It should be noted that the β-turn band component at 1681 cm^{-1} and the anti-parallel β-sheet band component at 1690 cm^{-1} showed only minor changes after the cells were exposed to the three compounds.

Fig. 6 shows the different pattern of the cell response to the three compounds in the protein region specifically the amide I band. FTIR spectroscopy indicated that all three test compounds induced apoptosis in varying degrees. This result suggests that the apoptosis effects in the U937 treated cells were related to a change of the β-sheet and α-helix of the protein structure. An increase of β-sheet structure of the apoptotic protein (Bax) was previously reported associated with apoptosis [18]. This study demonstrated that the three compounds exerted an anticancer activity based on apoptosis induction via pro-apoptotic proteins. It is, moreover, evidence that the amide I band (1700–1600 cm^{-1}) can be used as a FTIR marker for the apoptotic cells.

3.4. PCA analysis

The PCA was used to analyze the spread of the datasets acquired from the four different groups of the experiment. PCA was performed on the respective second derivative spectra from the 87, 54, 64, 55 spectra acquired from the untreated U937 cells and the melphalan-, *P. kesiya* extract- and *C. formosum* extract-treated U937 cells. The first three principal components (PCs) derived from the PCA classification of these spectra described more than 90% of the variance in the 4 experimental data sets (Fig. 7A). Four clusters of spectra from the untreated U937 cells, the U937 cells treated with the plant extracts and melphalan were clearly visualized in two dimensional score plots – PC1 vs. PC2 and PC2 vs. PC3 scores plots – from the PCA modeling (Fig. 7A).

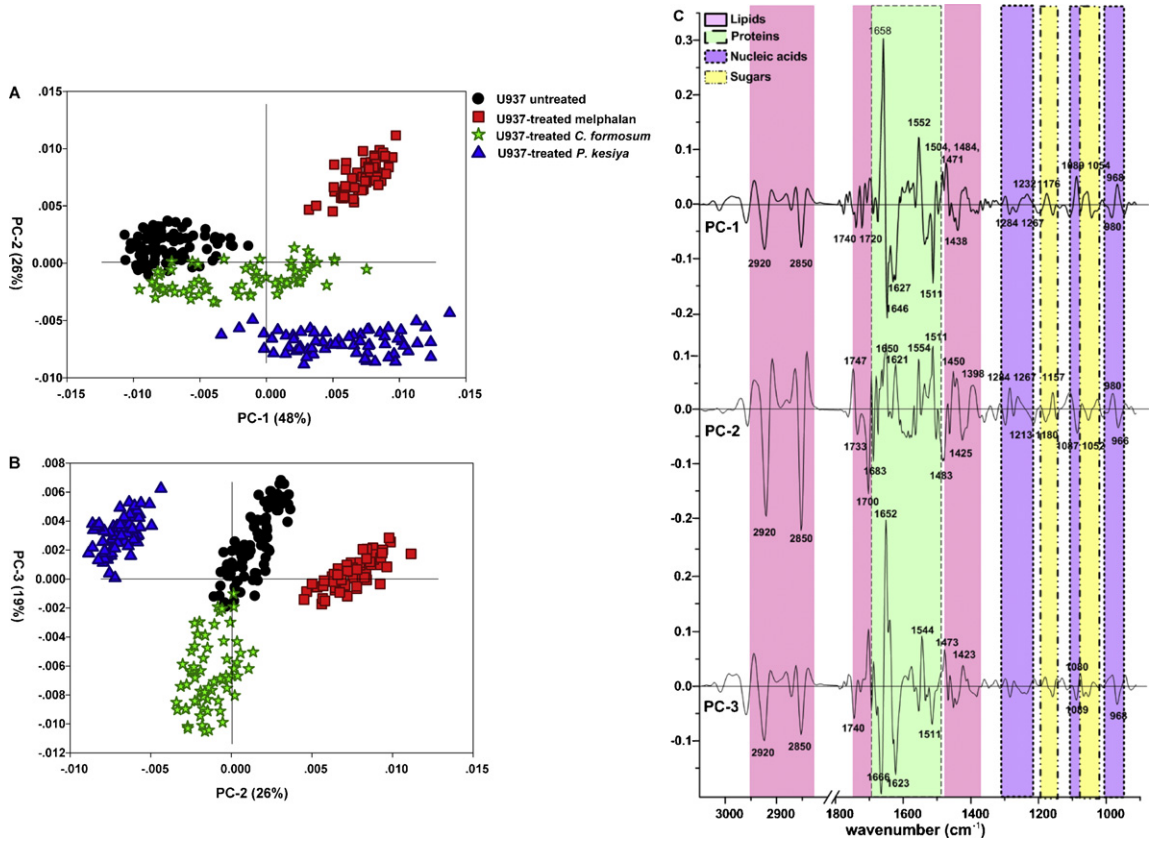

Fig. 7. PCA analysis of FTIR spectral range 3000–900 cm^{-1} giving PCA score plots (A and B) and PCA loading plots (C). PCA score plots showed distinct clustering between untreated U937 cells (●) and U937 treated with melphalan (■), *P. kesiya* extract (▲) and *C. formosum* (★) after 24 h exposure times. PCA loading plots indentify biomarker difference (i.e., discriminating wavenumbers) over spectral range of samples.

Fig. 7A and B clearly illustrate that the clusters of the untreated U937 cells were well separated from the clusters of *P. kesiya*- and melphalan-treated U937 cells along PC1 (48%) and the spectra of the melphalan- and *P. kesiya*-treated U937 cells were clustered separately along PC2 (26%). The spectra of the *C. formosum* were significantly distinct from the clusters of the untreated U937 cells and the melphalan- and *P. kesiya*-treated U937 cells along PC3 (19%). The three latter clusters caused similar alterations of the FTIR spectra (PC3) and were different from each other.

Analysis of the PCA loading plots (Fig. 7C) was used to determine the regions of the FTIR spectrum which most contributed to the clustering (Fig. 7A and B). The amide I band from proteins at 1658 cm^{-1} (assigned to the α-helix structure) was heavily loaded for PC1 which separated the negative score of the spectra of the untreated U937 cells from the positive score of the spectra of the melphalan- and *P. kesiya*-treated U937 cells (Fig. 7A). These data indicate that the α-helix structure (1658 cm^{-1}) band of the untreated cells was higher than the spectra of the melphalan- and *P. kesiya*-treated U937 cells. Moreover, the spectra from the melphalan- and *P. kesiya*-treated U937 cells could be distinguished from the untreated U937 cells by their having positive PC1 scores (Fig. 7A). This is perhaps because these spectra have the highest negative values of PC1 loading with variables between 1627 cm^{-1} and 1646 cm^{-1}, indicating that the respective β-sheet band of the melphalan- and *P. kesiya*-treated U937 cells was higher than the spectra of the untreated U937 cells. This indicates that the protein region at the α-helix band (1658 cm^{-1}) and the β-sheet band (1627 cm^{-1} and 1646 cm^{-1}) of PC1 are most strongly responsible for discriminating the melphalan- and *P. kesiya*-treated U937 cells from the untreated U937 cells, which was possibly attributable to the apoptotic proteins Bax and Bcl2 [22]. The negative of PC1 loading of the C–H stretching region (attributed to lipids band at 2921 cm^{-1} and 2852 cm^{-1}) could be due to an increase in lipids; since the PC1 positive scores discerned both melphalan and *P. kesiya* extract from the untreated U937 spectra.

The other high negative values of PC2 loading at 1700 and 1683 cm^{-1} also revealed that the β-turn structure [26] was responsible for discriminating between melphalan- and *P. kesiya*-treated U937 cells. The C–H stretching region assigned to the lipids (3000–2800 cm^{-1}) was heavily loaded for PC2, which separated the spectra of the melphalan-treated cells from that of the *P. kesiya*-treated cells (Fig. 7B). The melphalan-treated cells showed strong separation along positive PC2 scores, which were associated with the negative loading plot at 2921 and 2852 cm^{-1}. This result

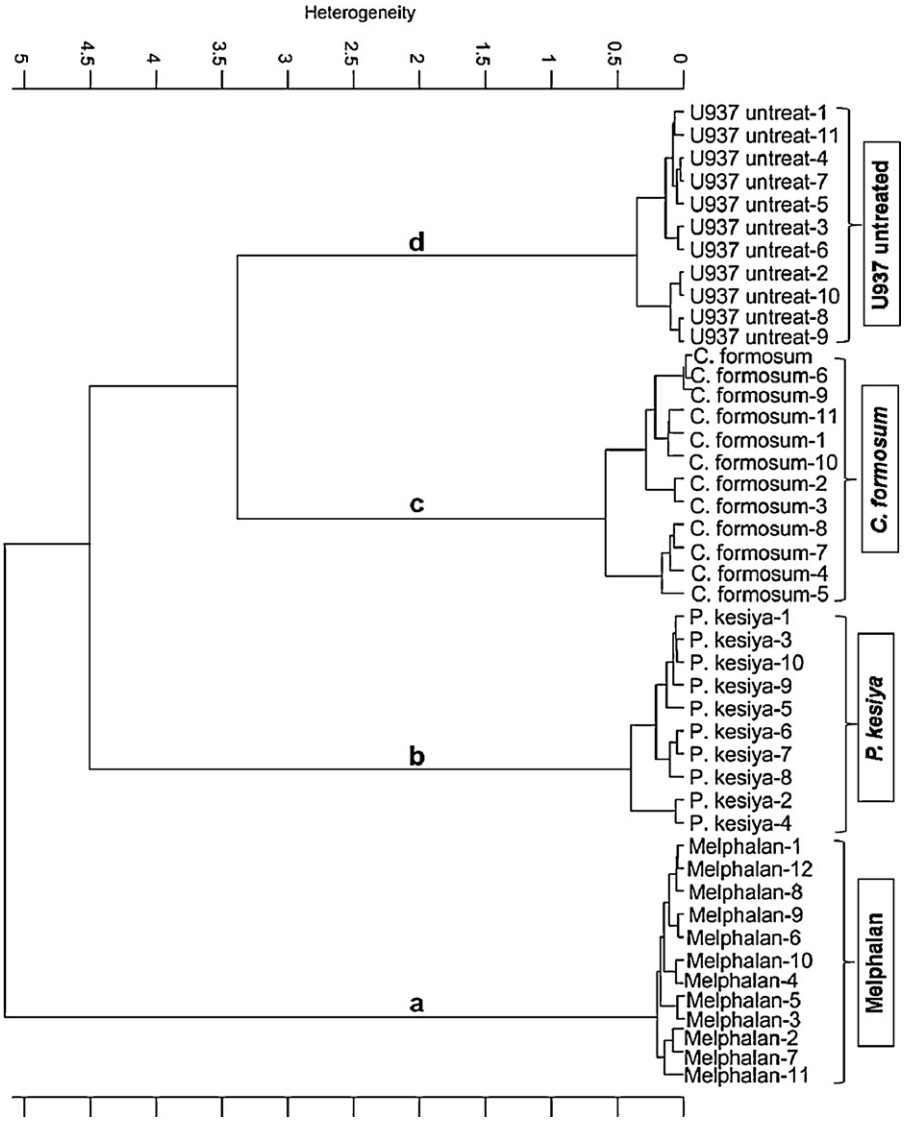

Fig. 8. Cluster classifications of infrared spectra of untreated U937 group and U937 treated groups (melphalan, *C. formosum* and *P. kesiya*) using same spectral data sets as in Fig. 4A. Classification based on Ward's algorithm. Distance between spectra significantly different at $P < 0.05$.

suggests that the U937 treated cells with melphalan had a higher lipid content than that of the *P. kesiya*-treated cells.

The spectra from the untreated cells and the *C. formosum*-treated U937 cells are likely to be co-localized along PC1 and PC2 (Fig. 7A). However, the clear separation was observed across the plotting of PC2 and PC3 (Fig. 7B). The spectra from the *C. formosum*-treated U937 cells are clearly separated by the negative correlation of the PC3 score (Fig. 7A), which have remarkably high positive PC3 loadings (Fig. 7B) at 1652 cm^{-1}; suggesting an α-helix protein structure in the *C. formosum*-treated U937 cells. It should be noted that the PC3 loading spectra at 1652 cm^{-1} was shifted from the 1658 cm^{-1} band of the untreated cells spectra. The negative of the PC3 loading of the C–H stretching region attributed to lipids band at 2921 and 2852 cm^{-1} could be interpreted as an increase in lipids since the PC3 positive scores discriminated the untreated U937 cells from the *C. formosum* extract-treated cells spectra.

In addition, the spectra of the nucleic acids region (*i.e.*, the phosphodiester groups and the C–O/C–C stretching of deoxyribose–ribose vibrations from the nucleic acids at 1089–966 cm^{-1}) were slightly loaded for PC1, PC2 and PC3. After consideration of the PC1, this band region separated the melphalan- and *P. kesiya*-treated U937 cells spectra from the untreated U937 cells spectra (Fig. 7C). The spectra from the melphalan- and, *P. kesiya*-treated U937 cells can be distinguished from the untreated U937 cells by having positive PC1 scores (Fig. 7A); according to the negative values of the PC1 loading at 968 and 1089 cm^{-1}, indicating that the DNA band is responsible for this discrimination [18]. The untreated U937 cells have a higher DNA content than the melphalan; as per the negative score plot (Fig. 7A) and the positive loading plot (Fig. 7C). The spectra of melphalan was separated from the spectra of the *P. kesiya*-treated U937 cells by having positive PC2 scores (Fig. 7B), corresponding to the negative values of the PC2 loading at 966 and 1087 cm^{-1} (Fig. 7C). Moreover, the spectra of the C. *formosum* was separated from the spectra of the melphalan- and *P. kesiya*-treated U937 cells and the untreated U937 cells by having negative PC3 scores (Fig. 7B), corresponding to the positive value of PC3 loading at 1080 cm^{-1} (Fig. 7C). Taken together the result of the PC1, PC2 and PC3 loading indicates that the DNA band is responsible for this cluster separation.

Based on the PCA analysis, the biochemical changes of the apoptotic U937 cells – associated with lipids, proteins and nucleic acids – as induced by three different compounds – can be discriminated from the untreated cells. The differences in intensity of the FTIR bands associated with lipids, proteins and nucleic acids were responsible for discrimination of the anticancer mode of action of each of the three compounds. All three compounds raised the intensity of the β-pleated sheet – higher than that of the untreated U937 cells – corresponding to a shift in the α-helix band associated with an alteration in the secondary structure of the protein band, confirming induction of apoptosis via pro-apoptotic proteins. At this point, we can confirm that the two plant extracts and melphalan display anticancer activity via apoptotic induction albeit through different mechanism.

3.5. Unsupervised hierarchical cluster analysis

Hierarchical cluster analysis (HCA) was performed to identify similarities and differences between spectra from the four different conditions studied – untreated cells, treated cells with melphalan, *P. kesiya* and *C. formosum* extracts – using spectral information in the lipid region (3000–2800 cm^{-1}) and the protein and nucleic acids region (1750–900 cm^{-1}), which were the regions of interest vis-à-vis the spectra of apoptotic cells. The Ward's linkage is a non-supervised method used for HCA analysis, which enables hierarchical clustering of groups with minimum loss of information; by taking account of the similarity of group members with respect to many variables [19,20].

The dendrogram in Fig. 8 visualizes the four major clusters of spectra. Evidently, the spectra within the lower branch *a* are clearly separated from the other branches; whereas the spectra from *P. kesiya* (in branch *b*) are separated from the two clusters corresponding to the spectra for *C. formosum* (in branch *c*), and the untreated U937 cells in branch *d*, respectively. The spectra of *C. formosum* in branch *c* are more similar to the untreated U937 cells in branch *d*. The statistical analysis of our data showed a significant difference ($P < 0.05$) between the U937 cells after being treated with melphalan and the *C. formosum* and *P. kesiya* extracts; indicating that each of the treated cell groups exhibited different modes of anticancer action via apoptotic processes based on their infrared spectral changes.

4. Conclusions

In conclusion, all three compounds – *C. formosum* ssp. *pruniflorum*, *P. kesiya* crude extracts and melphalan – possess anticancer activity against human leukemic U937 cells via an apoptosis death mode as indicated by morphological changes in the nuclei and DNA fragmentation. The anticancer drug melphalan exerts an anticancer activity via DNA alkylation and induction of DNA damage leading cancer cells to undergo apoptosis. FTIR microspectroscopy of the apoptotic U937 cells revealed that two plant extracts induced an apoptotic effect by a different mechanism. FTIR microspectroscopy was able to distinguish the mode of cell death, based on changes in the nucleic acid region (1300–900 cm^{-1}) and protein secondary structures (1700–1500 cm^{-1}), which are used as FTIR markers. The apoptosis effects of the three compounds were associated with a change in the β-sheet (1625–1618 cm^{-1}) and α-helix (1656–1650 cm^{-1}) of the protein structure. In our study, the lipid absorbance was not a good FTIR marker for identifying apoptosis. FTIR microspectroscopy proved to be a potential alternative method for identifying a signature of apoptosis induction of the test compounds on U937 cells using a non-destructive analysis of cell samples. Further detailed study should be done of the apoptosis induction mechanisms of the extracts of *P. kesiya* and *C. formosum* against U937 cells.

Conflict of interest

The authors declare that they have no conflicts of interest concerning this article.

Acknowledgements

SM was supported by The Office of the Higher Education Commission, Thailand, under the Strategic Scholarships for Thai Doctoral Degree Programs (CHE-PhD-THA-RG 3/2549). This research was also partially supported by the Plant Genetics Conservation Project under the Royal Initiation of Her Royal Highness Princess Maha Chakri Sirindhorn and by research funding from Khon Kaen University (511010815 and 520123). The authors would like to thank the Center for Research and Development of the Herbal Health Product, Khon Kaen University, for facilities, Assistant Professor Thaweesak Thitimetharoch for plant identification, and Mr. Bryan Roderick Hamman and Mrs. Janice Loewen-Hamman for assistance with the English-language presentation of the manuscript.

References

[1] J.A. Royle, P.D. Baade, D. Joske, J. Girschik, L. Fritschi, Br. J. Cancer 105 (2011) 1076–1081.

[2] B. Vogelstein, K.W. Kinzler, Nat. Med. 10 (2004) 789–799.
[3] H.J. Broxterman, N.H. Georgopapadakou, Drug Resist. Update 10 (2007) 182–193.
[4] N. Khan, V.M. Adhami, H. Mukhtar, Biochem. Pharmacol. 76 (2008) 1333–1339.
[5] T. Gallardo-Velazquez, G. Osorio-Revilla, M.Z. Loa, Y. Rivera-Espinoza, Food Res. Int. 42 (2009) 313–318.
[6] E.C. de Bruin, J.P. Medema, Cancer Treat. Rev. 34 (2008) 737–749.
[7] F. Brugnon, G. Verheyen, L. Janny, J. Pouly, I. Liebaers, A. Vansteirteghem, Fertil. Steril. 84 (2005), S61–S61.
[8] S. Rello, J.C. Stockert, V. Moreno, A. Gamez, M. Pacheco, A. Juarranz, A. Villanueva, Apoptosis 10 (2005) 201–208.
[9] R. Gasper, E. Goormaghtigh, Analyst 135 (2010) 3048–3051.
[10] H.Y.N. Holman, R. Miles, Z. Hao, E. Wozei, L.M. Anderson, H. Yang, Anal. Chem. 81 (2009) 8564–8570.
[11] A.A. Khan, M. Khalid, Synthetic Met. 160 (2010) 708–712.
[12] F. Gaspari, M. Muzio, Biochem. J. 369 (Pt 2) (2003) 239–248.
[13] A. Derenne, R. Gasper, E. Goormaghtigh, Analyst 136 (2011) 1134–1141.
[14] C. Gallardo-Escarate, J. Alvarez-Borrego, E. Von Brand, E. Dupre, M.A. Del Rio-Portilla, Biol. Res. 40 (2007) 29–40.
[15] S. Elmore, Toxicol. Pathol. 35 (2007) 495–516.
[16] E. Gazi, T.J. Harvey, M.D. Brown, N.P. Lockyer, P. Gardner, N.W. Clarke, Vib. Spectrosc. 50 (2009) 99–105.
[17] R. Gasper, J. Dewelle, R. Kiss, T. Mijatovic, E. Goormaghtigh, Biochim. Biophys. Acta 1788 (2009) 1263–1270.
[18] U. Zelig, J. Kapelushnik, R. Moreh, S. Mordechai, I. Nathan, Biophys. J. 97 (2009) 2107–2114.
[19] R. Gasper, T. Mijatovic, R. Kiss, E. Goormaghtigh, Appl. Spectrosc. 65 (2011) 584–594.
[20] R. Gasper, G. Vandenbussche, E. Goormaghtigh, Biochim. Biophys. Acta 1808 (2011) 597–605.
[21] P. Heraud, E.S. Ng, S. Caine, Q.C. Yu, C. Hirst, R. Mayberry, A.G Elefanty, Stem Cell Res. 4 (2010) 140–147.
[22] W. Tanthanucha, K. Thumanu, C. Lorthongpanich, R. Parnpai, P. Heraud, J. Mol. Struct. 967 (2010) 189–195.
[23] L. Di Giambattista, D. Pozzi, P. Grimaldi, S. Gaudenzi, S. Morrone, A.C. Castellano, Anal. Bioanal. Chem. 399 (2011) 2718–2771.
[24] A. Pukhalsky, G. Shmarina, V. Alioshkin, A. Sabelnikov, Biochem. Pharmacol. 72 (2006) 1432–1438.
[25] L.M. Miller, P. Dumas, Curr. Opin. Struct. Biol. 20 (2010) 649–656.
[26] P. Grimaldi, L. Di Giambattistaa, S. Giordania, I. Udroiub, D. Pozzi, S. Gaudenzi, A. Bedini, C. Giliberti, R. Palomba, A.C. Castellano, Spectrochim. Acta 84 (2011) 74–85.
[27] A. Ausili, A. Torrecillas, M.M. Martinez-Senac, S. Corbalan-Garcia, J.C. Gomez-Fernandez, J. Struct. Biol. 164 (2008) 146–152.
[28] K. Thumanu, W. Tanthanuch, D. Ye, A. Sangmalee, C. Lorthongpanich, R. Parnpai, P. Heraud, J. Biomed. Opt. 16 (2011) 057005.
[29] A. Torrecillas, M.M. Martinez-Senac, A. Ausili, S. Corbalan-Garcia, J.C. Gomez-Fernandez, Biochim. Biophys. Acta 1768 (2007) 2931–2939.